AIP Journal of Applied Physics

Microstructural, optical, and magnetic properties of Mn-implanted p-type GaN

Jeong Min Baik, Jong-Lam Lee, Yoon Shon, and Tae Won Kang

Citation: Journal of Applied Physics **93**, 9024 (2003); doi: 10.1063/1.1572974

View online: http://dx.doi.org/10.1063/1.1572974

View Table of Contents: http://scitation.aip.org/content/aip/journal/jap/93/11?ver=pdfcov

Published by the AIP Publishing

Microstructural, optical, and magnetic properties of Mn-implanted *p*-type GaN

Jeong Min Baik and Jong-Lam Lee[a)]
Department of Materials Science and Engineering, Pohang University of Science and Technology (POSTECH), Pohang, Kyungbuk 790-784, Korea

Yoon Shon and Tae Won Kang
Quantum Functional Semiconductor Research Center, Dongguk University, 3-26 Pil-dong, Chung-ku, Seoul 100-715, Korea

(Received 20 January 2003; accepted 17 March 2003)

The effect of microstructural change on both magnetic and optical properties of Mn-implanted *p*-type GaN was studied. A dilute magnetic semiconductor was achieved by implanting Mn ions into *p*-type GaN and subsequently annealing. The magnetization measurement showed that the Curie temperature was the highest in the 800 °C annealed sample due to the formation of Ga–Mn magnetic phases. The annealing at a higher temperature of 900 °C produced antiferromagnetic Mn–N compounds such as $Mn_6N_{2.58}$ and Mn_3N_2, leaving N vacancies. This provides evidence that N vacancies played a critical role in weakening the ferromagnetic property in the Mn-implanted GaN. The photoluminescence peak at 2.92 eV became strong after annealing at 800 °C, indicating an increase in hole concentration due to an enhanced activation of Mn impurities in *p*-type GaN. The intensity of Raman modes at 290 and 670 cm^{-1} decreased drastically as annealing temperature increased (>800 °C), due to the reduction in Mn-implantation-induced lattice imperfections. From this, it is proposed that the increase in magnetic properties of Mn-implanted GaN originated from the enhancement in the crystallinity as well as the production of Ga–Mn magnetic phases. © *2003 American Institute of Physics.* [DOI: 10.1063/1.1572974]

I. INTRODUCTION

Dilute magnetic semiconductors (DMSs) based on III–V semiconductors have attracted a great deal of attention because of their application to magnetic semiconductor devices such as spin-field effect transistors and spin-light emitting diodes.[1–3] For achieving high-quality performance of these devices, semiconductors with the Curie temperature T_C above room temperature are required. However, the reported T_C values for InMnAs, GaMnSb, and GaMnAs were lower than 110 K.[4–6]

(Ga,Mn)N is a very promising material because its T_C is higher than room temperature according to the theoretical calculation.[7] A GaN film ($\geqslant 10^{21}\,cm^{-3}$) heavily doped with Mn impurities, grown on sapphire (0001) by molecular beam epitaxy,[8] showed a ferromagnetic behavior. Mn-implanted and subsequently annealed GaN also showed the ferromagnetic property.[9,10] According to the material characterization using x-ray diffraction (XRD) and/or transmission electron microscopy, it was proposed that the solid solution of Mn in GaN and/or Ga–Mn binary phases would play a major role in emerging the ferromagnetic property in the Mn-doped GaN films. In the optical characterization of (Ga,Mn)N, photoluminescence (PL) peaks were observed at 2.5 and 3.0 eV in Mn-implanted and annealed GaN.[11] The Mn impurities in GaN, acting as a deep acceptor for electrons at an energy level of $E_v + 1.4\,eV$, played a role in strongly disordering the lattice structure.[12] Despite a number of works mentioned above, no experimental evidence on the effects of such secondary phases and lattice imperfections on both the ferromagnetic and optical properties in GaN-based DMS was provided because of lack of experimental resolution. The x-ray scattering and photoemission spectroscopy using synchrotron radiation could provide quantitative information about the chemical and electronic properties, which should be crucial for understanding the origin of ferromagnetic properties in GaN-based DMS. Combining the results with optical properties in the DMS films, one can understand the ferromagnetic properties with the changes in microstructural and optical properties.

In this work, we investigated microstructural, optical, and magnetic properties of Mn-implanted *p*-type GaN as a function of annealing temperature. Synchrotron XRD and synchrotron radiation photoemission spectroscopy (SRPES) were employed in order to study microstructural properties of Mn-implanted *p*-type GaN. The optical properties of samples were analyzed through photoluminescence spectroscopy and micro-Raman spectroscopy. From these results, the effect of microstructural change on both magnetic and optical properties of Mn-implanted *p*-type GaN is discussed.

II. EXPERIMENTAL PROCEDURE

The GaN films used in this work were grown by metal-organic chemical-vapor deposition on a (0001) sapphire substrate. An undoped GaN layer with a thickness of 1 μm was grown, followed by a growth of 1-μm-thick *p*-type GaN

a)Author to whom correspondence should be addressed; electronic mail: jllee@postech.ac.kr

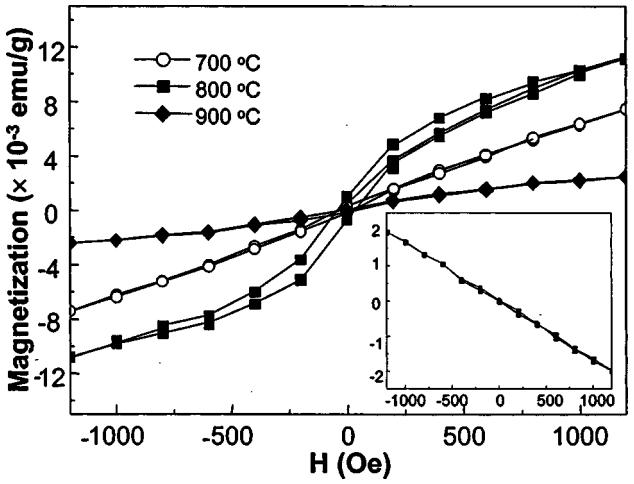

FIG. 1. Magnetization curves for Mn-implanted samples with various annealing temperatures. The inset shows the diamagnetic background of the as-grown *p*-type GaN.

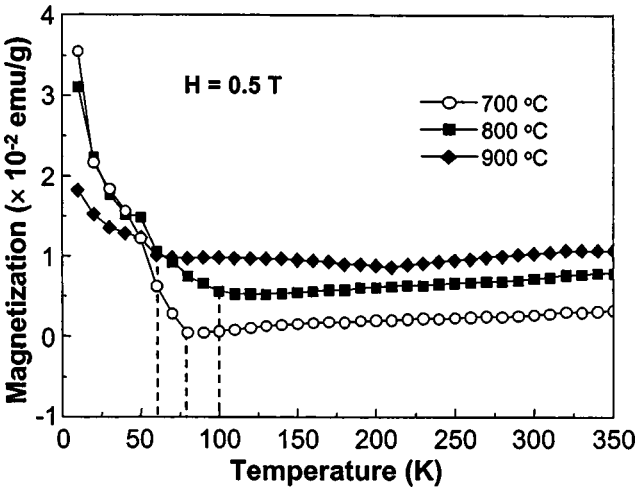

FIG. 2. Temperature dependent magnetization for Mn-implanted and annealed GaN. Samples were annealed at 700, 800, and 900 °C.

doped with Mg. Electrical activation of the grown samples was carried out at 750 °C for 4 min by rapid thermal annealing under N_2 atmosphere. Net hole concentration in the film was determined to be $2.5\times10^{17}\,\mathrm{cm}^{-3}$ by Hall measurements. After the growth of the films, Mn^+ ions were implanted into the *p*-type GaN films with an energy of 180 keV and the dose of $5\times10^{16}\,\mathrm{cm}^{-2}$. All samples were held at 350 °C during the implantation to avoid amorphization. Subsequent annealing at 700–900 °C for 30 s was performed under flowing N_2 gas in a face-to-face condition. Magnetization measurements were carried out using a superconducting quantum interference device magnetometer (MPMSXL, Quantum Design Co., Ltd).

High-resolution XRD and SRPES using synchrotron radiation were carried out at the 3C2 and 8A1 beamlines at Pohang Accelerator Laboratory (PAL). For high-resolution XRD measurements, the wavelength of incident x ray was set at 1.488 Å by a double bounce Si (111) monochromator. The energy resolution of binding energy in the SRPES measurements was ±0.05 eV. The binding energy of core level spectra was calibrated with the peak position of the Au $4f$ core level of an Au foil and that of the valence band spectra with the Fermi level of the Au foil. The measurements of Raman spectroscopy were performed at room temperature using an NRS-2100 spectrometer (JASCO, Japan) equipped with a triple-grating monochromator and a coherent Ar laser (Innova 90C) at 5145 Å. In the measurements, a micro-Raman option using an LN_2-cooled charge coupled device was used. The scattered light was detected in backscattering geometry. PL measurements were carried out using a 0.75 m monochromator equipped with an ultraviolet-sensitive photomultiplier. The excitation source was the 325 nm line of a He–Cd laser with the total power of 50 mW.

III. RESULTS

A. Magnetic properties

Figure 1 shows magnetization curves at 10 K for samples annealed at 700–900 °C. The magnetization curves were obtained with the applied field parallel to the plane of samples. The diamagnetic background of GaN layer was subtracted. The hysteresis loops showed clear ferromagnetic behavior of the samples. It was easily found that the ferromagnetic signal for the 800 °C annealed sample was the strongest among all annealed samples. With increasing annealing temperature, the coercive field (H_C) increased from 21 to 79 Oe. However, the residual magnetization (M_R) was the highest in the 800 °C annealed sample.

Temperature dependent magnetization ($M-T$) measurements were carried out up to 350 K at a constant applied magnetic field of $0.5T$, as shown in Fig. 2. Even though T_C is lower than the previously reported values,[8,10] the 800 °C annealed sample exhibited the highest T_C (100 K) among all annealed samples. The temperature dependency of magnetic moment showed an anomalous increase and discontinuous change below about 70 K. This supports that Mn-related compounds or alloys were included in the present samples.

B. Microstructural analysis

Figure 3(a) shows XRD profiles of Mn-implanted GaN samples with various annealing temperatures. Compared to

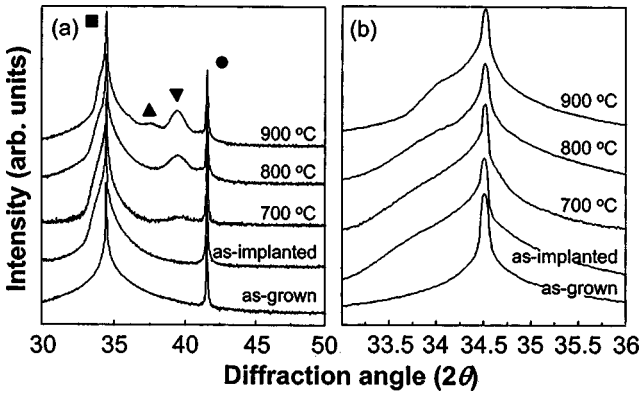

FIG. 3. (a) Change of XRD scans for the Mn-implantated GaN with the annealing temperature. (b) Expanded view at around GaN (0002) peak; (■) GaN, (●) Al_2O_3, (▼) $Mn_6N_{2.58}$, (▲) Mn_3N_2.

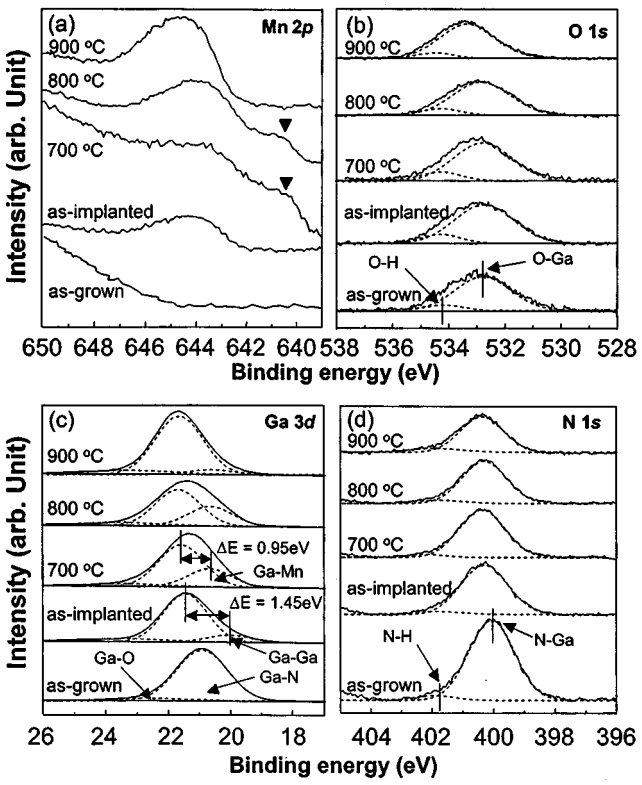

FIG. 4. Change of SRPES spectra for (a) Mn $2p_{3/2}$, (b) O 1*s*, (c) Ga 3*d*, and (d) N 1*s* core levels in Mn-implantated GaN with various annealing temperatures.

the as-grown sample, no reaction between Mn and GaN was observed in the as-implanted one. After annealing at 700 °C, the Mn–N binary phase of $Mn_6N_{2.58}$ was produced. The $Mn_6N_{2.58}$ peak intensity increased with the annealing temperature. When the sample was annealed at 900 °C, a new peak corresponding to Mn_3N_2 was observed. Figure 3(b) shows enlarged XRD scans ranging from $2\theta=33°$ to 36°. A shoulder was found at the lower angle side of GaN (0002) peak and its intensity became larger at higher annealing temperature. The shoulder could attribute to the strain along the GaN *c* axis, resulting from the decrease of implantation-induced damage during the annealing.[13]

Figure 4 shows the change of SRPES spectra of Mn $2p_{3/2}$, O 1*s*, Ga 3*d*, and N 1*s* core levels with annealing temperature. In order to remove surface oxides, the samples were *in situ* etched about 50 Å using Ar ion sputtering. Only one peak was observed in the Mn $2p_{3/2}$ spectra for both as-implanted and 900 °C annealed samples, as shown in Fig. 4(a). The peak could be either an Mn–N bond or a Mn–O bond. As annealing temperature increased, the peak intensity became larger. In Fig. 4(b), it is apparently found that the intensity of O 1*s* peak is independent of annealing temperature. This means that the main peak in Fig. 4(a) corresponds to the Mn–N bond rather than the Mn–O one. The presence of Mn–N bond is in good agreement with the XRD data in Fig. 3. In the samples annealed at 700 and 800 °C, a new peak was located at a binding energy of 640.5 eV, lower by ~3.0 eV than the Mn–N binding energy. This could be either metallic Mn–Mn[14] or Ga–Mn bonds. The origin of the peak was revealed by the SRPES spectra of Ga 3*d*, shown in Fig. 4(c). The Ga 3*d* spectrum of the as-grown sample consists of Ga–N and Ga–O bonds. After the Mn implantation, the spectrum showed asymmetry at the lower bonding energy of the Ga–N bond. The full width at half maximum (FWHM) value of the Ga 3*d* peak was measured to be 1.65 eV for the as-grown *p*-type GaN, but 1.95 eV for the 800 °C annealed *p*-type GaN. This means that an additional bonding is superimposed in the Ga 3*d* spectra. For the Mn-implanted sample, the superimposed peak could be attributed to metallic Ga atoms in GaN due to the implantation-induced loss of nitrogen atoms.[14] The difference of binding energy between Ga–N and Ga–Ga bonds is in good agreement with the reported value of 1.7 eV.[15] For the sample annealed at 700 and 800 °C, a new peak could be separated at the lower bonding energy by 0.95 eV relative to the peak of Ga–N bonds. The Ga atoms in the Mn-implanted sample could make bonds with N, O, and Mn atoms, corresponding to Ga–N, Ga–O, and Ga–Mn bonds, respectively. Considering the electron negativity of each element, the Ga–Mn bond should locate between the Ga–N and Ga–Ga bonds.[15] Thus, the new peak should originate from the Ga–Mn bond. After annealing at 900 °C, the peak intensity for the Ga–Mn bond decreased drastically. FWHM values and relative concentrations of deconvoluted peaks in the Ga 3*d* spectra are summarized in Table I. Meanwhile, the N 1*s* spectrum consists of N–H and N–Ga bonds, as shown in Fig. 4(d). With annealing temperature, the N 1*s* peak intensity decreased.

TABLE I. Relative concentrations (%) of chemical bonds determined from the Ga 3*d* SRPES spectra in Fig. 3(b). The values in parentheses represent FWHM value of each bond.

Sample	Ga–N (1.52 eV)	Ga–O (2.71 eV)	Ga–Ga (1.42 eV)	Ga–Mn (1.50 eV)
As grown	91.2	8.8	···	···
As implanted	81.9	10.1	8.0	···
700 °C	69.2	10.4	···	20.5
800 °C	63.4	10.3	···	26.3
900 °C	78.9	13.0	···	8.1

The relative atomic ratio of Ga/N was determined from integrating intensities in the Ga 3*d* [Fig. 4(c)] and N 1*s* spectra [Fig. 4(d)], plotted in Fig. 5. The ratio measured at a detection angle of $\theta=90°$ in the as-implanted sample was set as 1.0 for reference. As annealing temperature increased, the Ga/N ratio increased, indicating the production of N vacancies in the annealed GaN. At a smaller θ, the intensity of photoelectrons emitting from the surface becomes dominant due to the inelastic mean-free path of photoelectrons. At $\theta=30°$, the increase of the Ga/N ratio with annealing temperature was more pronounced. This supports the fact that nitrogen atoms were preferentially diffused out to the surface during the annealing, leaving N vacancies near the surface region.

The change of surface band bending with annealing temperature was observed from valence band spectra, as shown in Fig. 6. The Fermi level was determined by linearly extrapolating the sloped region to the base line in the valence band spectrum of a Au foil, defined as the level of zero binding energy (E_F). For the sample annealed at 900 °C, the

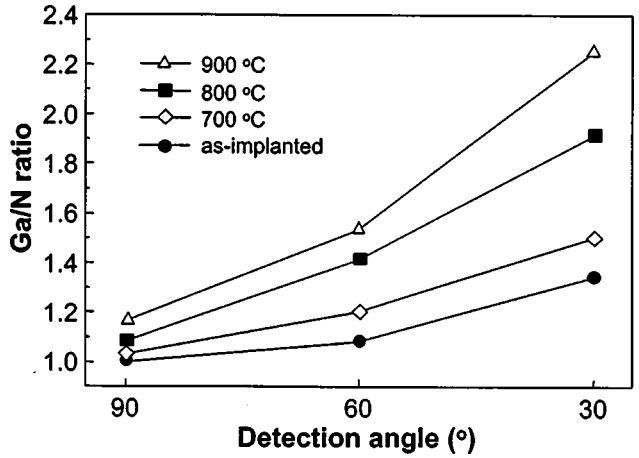

FIG. 5. Change of Ga/N atomic ratio of Mn-implanted GaN with various annealing temperatures.

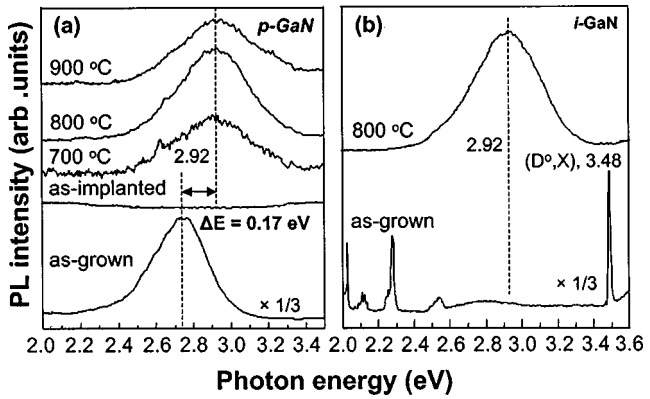

FIG. 7. (a) PL spectra at 10 K for as-grown, as-implanted, and annealed samples at 700, 800, and 900 °C. (b) PL spectra at 10 K for as-grown and 800 °C annealed undoped GaN samples.

Fermi level shifted by 0.5 eV toward conduction band in comparison with the as-implanted sample. This is related to N vacancies produced during the annealing[14] because N vacancies act as donors for electrons.[16] However, after annealing at 700 and 800 °C, the Fermi level nearly coincides with the valence band maximum. This is due to the fact that the surface of the Mn-implanted sample changed into metallic surface, consistent with the observation of metallic Ga–Mn bonds in Figs. 4(a) and 4(c).

C. Optical properties

Figure 7(a) shows PL spectra of Mn-implanted *p*-type GaN samples as a function of annealing temperature. For the as-grown sample, the transition related to Mg acceptors appeared at the energy of 2.75 eV without yellow luminescence transition. No PL signal was observed in the as-implanted sample due to an abundance of implantation-induced imperfections. After annealing at 700 °C, a peak with a broad blue band occurred at 2.92 eV. The PL signal became more intense with annealing temperature and showed a maximum at 800 °C. Further increase in annealing temperature to 900 °C resulted in a decrease in the PL intensity. In order to clarify the origin of the 2.92 eV peak, Mn ions were implanted into undoped GaN and subsequently annealed at 800 °C under the same condition. The resultant PL spectra were displayed in Fig. 7(b). The 2.92 eV emission line was also observed in undoped GaN. This supports the fact that the transition at 2.92 eV is not related to the Mg impurity in *p*-type GaN, but apparently originates from the Mn impurities in GaN.

Figure 8 shows the temperature dependence of the blue band for the Mn-implanted sample annealed at 800 °C. With increasing temperature, the blue band shifted to the lower energy (~25 meV at 300 K) Conduction band to acceptor (e-A) transition is given by[17]

$$E_{eA} = E_g - E_A + 1/2k_BT, \tag{1}$$

where, k_B is the Boltzmann constant, E_g, the band gap energy, E_A, the acceptor energy level, and T is the temperature. It is clearly found that the e-A transition shifts to the higher energies with increasing temperature. This indicates that the blue band of 2.92 eV cannot be explained by e-A transition. Therefore, the distinct shift of the 2.92 eV blue band to the lower energy is a clear indication for the recombination of

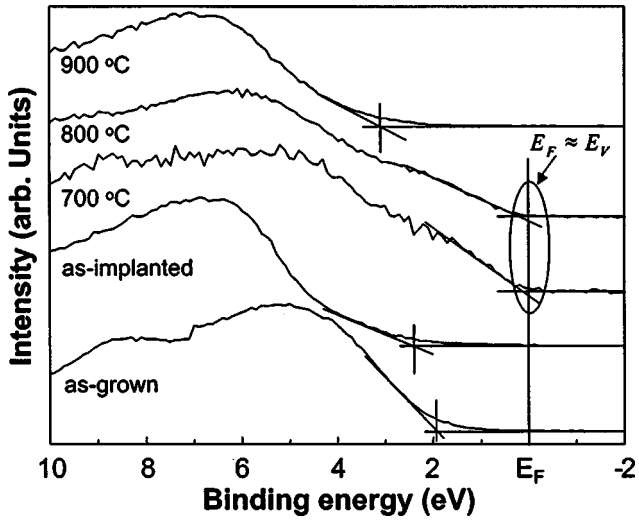

FIG. 6. Change of valence band spectra of Mn-implanted GaN with various annealing temperatures.

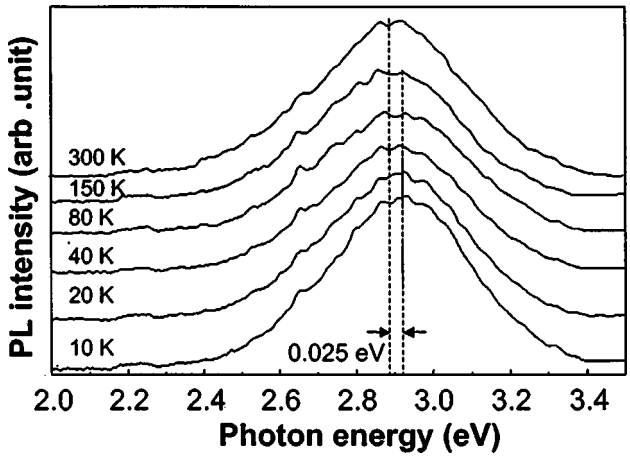

FIG. 8. Temperature dependence PL spectra of a sample annealed at 800 °C. The inset shows the change of the peak energy with device temperature.

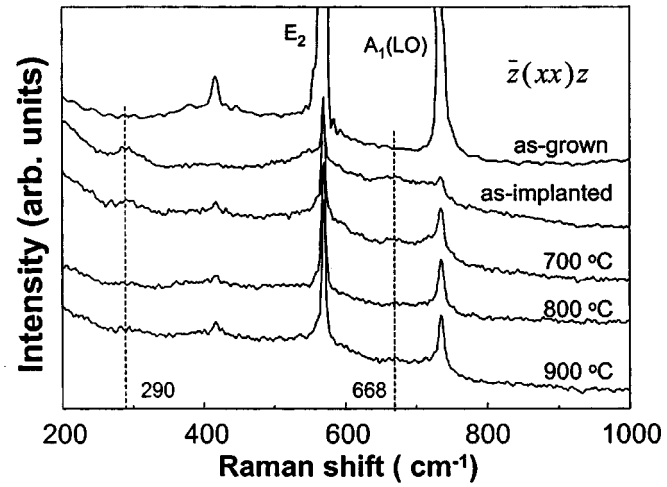

FIG. 9. Raman spectra of Mn-implanted samples as a function of annealing temperature. The measurements were carried out at room temperature.

electrons with holes trapped at spatially separated donors and acceptors, that is, the nature of donor–acceptor pair.

Figure 9 shows Raman spectra for the Mn-implanted GaN samples with various annealing temperatures. For the as-grown sample, two lines corresponding to the E_2 and A_1 longitudinal optical (LO) modes were observed as expected from the Raman selection rules in wurzite GaN films.[18] The weak line at 418 cm^{-1} stems from the sapphire substrate. After the Mn implantation, the intensities of the E_2 and A_1 LO modes decreased and two additional peaks occurred at wave numbers of 290 and 670 cm^{-1}. Whereas the intensities of the E_2 and A_1 LO modes increased with annealing temperature, the intensities of the modes at 290 and 670 cm^{-1} decreased. In particular, a high temperature annealing above 800 °C showed a drastic decrease in intensities of the modes. In the previous work on Raman spectroscopy for ion-implanted GaN films, the modes at 290 and 670 cm^{-1} appeared in samples implanted with Ar, Mg, P, C, and Ca ions.[19] This means that such modes are independent of the local vibrations of Mn impurities. Therefore, it is believed that these modes at 290 and 670 cm^{-1} originated from the macroscopic disorder or vacancy-related defects due to the Mn implantation.

IV. DISCUSSION

A. Correlation between magnetic properties and microstructure

In the SRPES measurements, the peak corresponding to Ga–Mn bonds was observed in the 700 and 800 °C annealed samples [Fig. 4(c)]. But the peak intensity for the Ga–Mn bonds significantly decreased and the ferromagnetic signal also decreased as annealing temperature increased to 900 °C [Fig. 1]. Based on the results reported previously that the ferromagnetic behavior of Mn-implanted GaN could be due to the formation of Mn_3Ga phase,[10] it is proposed that the Ga–Mn bond found after annealing 700 and 800 °C [Fig. 4(c)] contributed to the ferromagnetic property [Figs. 1 and 2].

Meanwhile, the Ga–Mn phases could not be identified in the XRD measurements [Fig. 3]. No observation of such Ga–Mn phases might be attributed to the nano-scale size[10] and random orientation of the Ga–Mn magnetic phases. The Ga–Mn magnetic phases reduced drastically as annealing temperature increased to 900 °C. This is due to the fact that Mn preferentially interacted with N atoms to precipitate the Mn–N binary phases of Mn_3N_2 and $Mn_6N_{2.58}$, as shown in Fig. 3. Since the Mn–N compounds are antiferromagnetic materials with Néel temperature above 300 K,[20,21] the magnetic moment of the Mn-implanted GaN was reduced by the formation of the Mn–N compounds.

B. Correlation between magnetic properties and Mn-induced defects

In XRD measurements, the formation of Mn_3N_2 and $Mn_6N_{2.58}$ phases was pronounced after the higher annealing temperature at 900 °C. This formation of Mn nitrides in GaN should change surroundings into N-deficient condition, leading to the formation of N vacancies. This is supported by the result that the Ga/N ratio at $\theta=90°$ increased with annealing temperature [Fig. 5]. In GaN films, N vacancies have shallow donor levels, located at about 30–40 meV below the conduction band edge.[17] Thus, some part of the holes compensates with electrons generated from N vacancies, leading to the reduction of hole concentration. It was reported that the holes mediate the long-range interactions between the localized spins in the III–V magnetic semiconductors, enhancing ferromagnetic properties of the materials.[1] Therefore, ferromagnetic signal reduced as the concentration of N vacancies increased.

The Mn-related PL band was observed at 2.92 eV as the Mn-implanted sample was annealed [Fig. 7(a)]. Because Mn impurities in III–V compounds act as acceptors for electrons, it is suggested that the blue emission at 2.92 eV is due to the recombination of donors such as N vacancies and Mn acceptors. It is worth noting that the peak intensity in the 800 °C annealed sample, where the strongest ferromagnetic signal was observed, was the largest among the annealed samples. In a photoexcitation process, excess carriers play an important role since the donor-to-acceptor pair recombination probability is determined by the number of donors and acceptors.[22] The increase in Mn acceptor centers would increase the probability of holes being captured to form donor-to-acceptor pairs, resulting in larger PL peak intensity. From this, it is suggested that the increase in the activation of Mn atoms in the 800 °C annealed sample resulted in the production of radiative Mn centers responsible for the donor-to-acceptor pair transition. Meanwhile, the intensity of the emission peak for 900 °C annealed samples reduced [Fig. 7(a)]. This could be attributed to the minor surface decomposition during the high temperature annealing, leading to the degradation of PL signals.[23]

The production of lattice imperfections in Mn-implanted and annealed samples could be deduced from Raman spectra, as shown in Fig. 9. The intensities of Raman modes observed at 290 and 690 cm^{-1} in the Mn-implanted GaN decreased with the annealing temperature. In particular, the decrease was pronounced after annealing above 800 °C. The modes

were due to macroscopic disorders or vacancy-related defects in the ion-implanted GaN sample, not the local vibration of implanted atoms.[19] Thus, it is suggested that annealing the implanted GaN at temperatures higher than 800 °C resulted in the reduction of implantation-induced disorders in Mn-implanted GaN films, improving magnetic properties of the films. Consequently, it is suggested that optimum annealing temperature (<900 °C) could be an important parameter in enhancing the ferromagnetism in the Mn-implanted and annealed GaN by suppressing the production of N vacancies

V. CONCLUSION

In this work, dilute magnetic semiconductor was achieved by implanting Mn ions into *p*-type GaN and subsequently annealing. The Ga–Mn magnetic phases contributing to the ferromagnetic property were produced after annealing Mn-implanted *p*-type GaN below 800 °C. Increasing the annealing temperature to 900 °C promoted the formation of antiferromagnetic Mn–N compounds such as $Mn_6N_{2.58}$ and Mn_3N_2, leaving N vacancies. In PL measurements, the emission intensity of the Mn-related photoluminescence peak at 2.92 eV was stronger after annealing at 800 °C, indicating the generation of higher hole concentration due to an effective Mn activation. The intensities of Raman modes at 290 and 670 cm^{-1} due to macroscopic disorder or defects decreased drastically after annealing above 800 °C. This means that high temperature annealing (>800 °C) was required for high crystal quality of the Mn-implanted sample. In these results, it is suggested that ferromagnetic properties of Mn-implanted *p*-type GaN could be enhanced by optimizing annealing temperature (~800 °C).

ACKNOWLEDGMENTS

This work was supported in part by the Korea Science and Engineering Foundation through the Quantum-Functional Semiconductor Research Center at Dongguk University in 2003, and in part by the project for ''National Research Laboratory'' sponsored by the Korea Institute of Science and Technology Evaluation and Planning (KISTEP). High-resolution XRD and SRPES using synchrotron radiation were carried out at the 3C2 and 8A1 SPEM beamlines at the Pohang Accelerator Laboratory (PAL), respectively.

[1] H. Ohno, Science (Washington, DC, U.S.) **281**, 951 (1998).
[2] H. Ohno, A. Shen, F. Matsukura, A. Oiwa, A. Endo, S. Katsumoto, and Y. Iye, Appl. Phys. Lett. **69**, 363 (1996).
[3] M. L. Reed, N. A. El-Masry, H. H. Stadelmaier, M. K. Ritums, M. J. Reed, C. A. Parker, J. C. Roberts, and S. M. Bedair, Appl. Phys. Lett. **79**, 3473 (2001).
[4] A. Oiwa, T. Slupinski, and H. Munekata, Appl. Phys. Lett. **78**, 518 (2001).
[5] K. Takamura, F. Matsukura, D. Chiba, and H. Ohno, Appl. Phys. Lett. **81**, 2590 (2002).
[6] F. Matsukura, E. Abe, and H. Ohno, J. Appl. Phys. **87**, 6442 (2000).
[7] T. Diel, H. Ohno, F. Matsukura, J. Cibert, and D. Ferrand, Science (Washington, DC, U.S.) **287**, 1019 (2000).
[8] S. Sonoda, S. Shimizu, T. Sasaki, Y. Yamamoto, and H. Hori, J. Cryst. Growth **237/239**, 1358 (2002).
[9] Y. Shon, Y. H. Kwon, D. Y. Kim, X. Fan, D. Fu, and T. W. Kang, Jpn. J. Appl. Phys., Part 1 **40**, 5304 (2001).
[10] N. Theodoropoulou, A. F. Hebard, M. E. Overberg, C. R. Abernathy, S. J. Pearton, S. N. G. Chu, and R. G. Wilson, Appl. Phys. Lett. **78**, 3475 (2001).
[11] R. Y. Korotkov, J. M. Gregie, and B. W. Wessels, Appl. Phys. Lett. **80**, 1731 (2002).
[12] W. Gebicki, G. Kamler, T. Szyszko, S. Podsiadlo, and J. Strzeszewski, Appl. Phys. Lett. **76**, 3870 (2000).
[13] B. J. Pong, C. J. Pan, Y. C. Teng, G. C. Chi, W.-H. Li, K. C. Lee, and C.-H. Lee, J. Appl. Phys. **83**, 5992 (1998).
[14] Y. Nakano and T. Kachi, Appl. Phys. Lett. **79**, 1468 (2001).
[15] J. F. Mouler, W. F. Strickle, P. E. Sobol, and K. D. Bomben, *Handbook of X-Ray Photoelectron Spectroscopy* (Perkin-Elmer, Eden Prairie, MN, 1992).
[16] P. Boguslawski, E. L. Briggs, and J. Bernholc, Phys. Rev. B **51**, 17255 (1995).
[17] S. Fisher, C. Wetzel, E. E. Haller, and B. K. Meyer, Appl. Phys. Lett. **67**, 1298 (1995).
[18] M. Cardona, in *Light Scattering in Solids II*, edited by M. Cardona and G. Güntherodt (Springer, Berlin, 1982), Vol. 50.
[19] W. Limmer, W. Ritter, R. Sauer, B. Mensching, C. Liu, and B. Rauschenbach, Appl. Phys. Lett. **72**, 2589 (1998).
[20] H. Yang, H. Al-Brithen, E. Trifan, D. C. Ingram, and A. R. Smith, J. Appl. Phys. **91**, 1053 (2002).
[21] M. N. Eddine and E. F. Bertaut, Solid State Commun. **23**, 147 (1977).
[22] L. S. Wang, W. K. Fong, C. Surya, K. W. Cheah, W. H. Zheng, and Z. G. Wang, Solid-State Electron. **45**, 1153 (2001).
[23] S. Nakamura, T. Mukai, M. Senoh, and N. Iwasa, Jpn. J. Appl. Phys., Part 2 **31**, L139 (1992).